JOURNAL OF VIROLOGY, Feb. 1986, p. 578–584
0022-538X/86/020578-07$02.00/0

Vol. 57, No. 2

Hexavalent Capsomers of Herpes Simplex Virus Type 2: Symmetry, Shape, Dimensions, and Oligomeric Status

ALASDAIR C. STEVEN,[1]* CHESTER R. ROBERTS,[2] JOHN HAY,[2] MARGARET E. BISHER,[1] THIERRY PUN,[3] AND BENES L. TRUS[4]

Laboratory of Cellular and Developmental Biology, National Institute of Arthritis, Diabetes and Digestive and Kidney Diseases,[1] and Biological Engineering and Instrumentation Branch,[3] and Computer Systems Laboratory, Division of Computer Research and Technology,[4] National Institutes of Health, Bethesda, Maryland 20892; and Microbiology Department, Uniformed Services University of the Health Sciences, 4801 Jones Bridge Road, Bethesda, Maryland 20814[2]

Received 5 August 1985/Accepted 23 October 1985

The structures of the hexavalent capsomers of herpes simplex virus type 2 were analyzed by negative staining electron microscopy of capsomer patches derived from partially disrupted nucleocapsids. Optimally computer-averaged images were formed for each of the three classes of capsomer distinguished by their respective positions on the surface of the icosahedral capsid with a triangulation number of 16; in projection, each capsomer exhibited unequivocal sixfold symmetry. According to correspondence analysis of our set of capsomer images, no significant structural differences were detected among the three classes of capsomers, as visualized under these conditions. Taking into account information from images of freeze-dried, platinum-shadowed nucleocapsid fragments, it was established that each hexavalent capsomer is a hexamer of the 155-kilodalton major capsid protein. The capsomer has the form of a sixfold hollow cone ~12 nm in diameter and ~15 nm in depth, whose axial channel tapers in width from the outside towards the inner capsid surface.

A full understanding of the assembly mechanisms that specify the clustering of protein subunits to form viral capsids is still lacking. According to the theory of quasiequivalence (5), the capsomers (oligomers of capsid protein[s]; hexavalent [pentavalent] capsomers are surrounded by 6 [5] other capsomers) should be arrayed on icosahedral surface lattices, with 12 pentavalent capsomers occurring at the vertices and hexavalent capsomers occupying the intervening spaces. Such icosahedra are classified by triangulation numbers (T) in the series T = 1, 3, 4, 7, etc., and contain increasing numbers [10 × (T − 1)] of hexavalent capsomers (5). A further provision of this theory is that the pentavalent and hexavalent capsomers should be pentamers and hexamers, respectively, of the same protein. As experimental evidence has accumulated, it has become clear that icosahedral surface lattices are indeed almost ubiquitous (21). However, in an increasing number of cases, capsomer organization has turned out to be other than that given above, particularly among the double-stranded DNA-containing animal viruses. For example, the hexavalent capsomers of adenovirus (T = 25) are trimers (4, 7), whereas adenovirus pentavalent capsomers contain a different protein, which also has been reported to be trimeric (8). The hexavalent capsomers of Frog Virus 3, an iridovirus with a T number of ~133, are also thought to be trimers (F. Darcy-Tripier, M. V. Nermut, E. Brown, H. Nonnenmacher, and J. Braunwald, Virology, in press). On the other hand, the hexavalent capsomers of polyomavirus (T = 7) have been found to be pentamers, like its pentavalent capsomers (3, 20). As yet, no empirical trend or theoretical insight has emerged which allows the prediction of the type of capsomer(s) to be expected for any given virus on the basis of other more fundamental properties. In this context, we have investigated the capsomer structure of herpes simplex virus type 2 (HSV-2), a representative member of the herpesvirus family.

* Corresponding author.

The surface lattice of the herpes simplex virus capsid has long been known to be a T = 16 icosahedron (31), but the composition of its capsomers has been a matter of unresolved debate. Several electron microscopic studies of negatively stained nucleocapsids have argued that the hexavalent capsomers are hexamers (1, 11, 19), but it has also been proposed on the basis of the same type of evidence (29) that they are trimers. The latter possibility would conform to the precedent established in adenovirus, whereas it has not yet been shown conclusively that any animal viruses have hexameric capsomers. However, interpretation of such images is complicated by the variability in staining conditions, the superposition of details from the upper and lower surfaces, and other factors that contribute to an adverse signal-to-noise ratio. Image-processing techniques, based on image averaging implemented in various forms (18), offer a potential solution to these problems. In this study we performed negative staining electron microscopy of patches of HSV-2 capsomers derived from disrupted capsids and made a computational analysis of them by correlation averaging and correspondence analysis (9, 28). These procedures admit the formation of optimally averaged images that are properly corrected for spatial disordering effects and allow their statistical classification. In addition, we prepared HSV-2 nucleocapsids for electron microscopy by freeze-drying and shadowing. The resulting images complement the negative staining data, allowing a proposal to be made for the three-dimensional organization of the hexavalent capsomers.

MATERIALS AND METHODS

Cells and virus. The human foreskin fibroblast line USU 184 (a gift of G. Fischer, Department of Pediatrics, Uniformed Services University of the Health Sciences) was grown in Eagle minimal essential medium supplemented with gentamicin (100 μg/ml) and 10% fetal calf serum. HSV-2 (strain HG 52 (26) was grown on confluent monolayers of 184 cells with a multiplicity of infection of 0.05 PFU per cell. Stock virus was prepared by scraping infected monolayers after about 3

days at 37°C, disrupting the cells with ultrasonic treatment, and titrating by the method of Russell (22).

Preparation of nucleocapsids. Nucleocapsids were prepared from infected 184 cells by the method of Straus et al. (25). Infected cell monolayers were washed twice with phosphate-buffered saline at 4°C and then scraped and pelleted at 1,500 × *g* for 5 min. The cell pellet was put through a cycle of freezing in a slurry of dry ice-acetone and thawing at 37°C three times and was then suspended in lysis buffer (0.5% Nonidet P-40, 3.6 mM $CaCl_2$, 5 mM magnesium acetate, 125 mM KCl, 0.5 mM EDTA, 6 mM 2-mercaptoethanol, 0.5% deoxycholate, [pH 7.5]). To each 1 ml of lysis buffer were added 25 μg of DNase and 25 μg of RNase, and incubation was carried out at 37°C for 30 min. The solution was then shaken for 1 min with an equal volume of trichlorotrifluoroethane, and the aqueous phase was layered over a 5 to 40% discontinuous glycerol gradient in lysis buffer. After 45 min at 105,000 × *g*, the pellet was suspended in 10 mM Tris hydrochloride–1 mM EDTA (pH 7.5; TE buffer).

Disruption of nucleocapsids: limited proteolysis with trypsin. Fractions (50 μl) of each of the nucleocapsid suspensions described above each were mixed with 50 μl of phosphate-buffered saline containing 9 U of trypsin (Worthington Diagnostics, Freehold, N. J.) activity and incubated at 37°C for various times (2 min in the case of samples which produced the most patches of capsomers for electron microscopy). The reaction was stopped by the addition of 150 μl of aprotinin (Sigma Chemical Co., St. Louis, Mo.) followed by centrifugation at 4°C in a Beckman microfuge B for 5 min. The pellet was suspended in 50 μl of TE buffer.

Electron microscopy. Specimens were negatively stained by applying a drop of nucleocapsid suspension for 60 s to a 400-mesh copper grid bearing a nitrocellulose substrate covered with a thin layer of carbon. The grid was washed twice with drops of TE buffer and stained for 15 s with 1% uranyl acetate. The excess stain was drawn off with Whatman no. 3 filter paper, and the grid was allowed to dry.

Freeze-drying and shadowing were performed essentially as described by Kistler et al. (14). A suspension of particles in TE buffer was adsorbed for 60 s to a carbon-coated, nitrocellulose-backed support film, which was then washed (four cycles) with double-distilled water. The grid was immersed in liquid nitrogen, placed (while submerged) on a grid holder with a protective lid, and transferred to the specimen holder of a Balzers BAF300 freeze-etch unit that had been precooled to −196°C. The unit was immediately evacuated, and the specimens were freeze-dried for 30 min at −100°C, followed by 15 min at −50°C. For unidirectional shadowing, the specimen was returned to −80°C, and platinum was deposited from an elevation angle of 30° to an average thickness of 1 nm as measured with a quartz crystal monitor (Balzers QSG201). Finally, a thin layer of carbon was evaporated onto the specimens.

Electron microscopy was performed with Philips EM400T and EM300 microscopes operating at 80 kV. A liquid nitrogen anticontamination device was used routinely. Nominal magnifications were ×36,000 and ×46,000, and these were calibrated by using the 2.49-nm periodicity of crystallites of the dye Olive-T (15).

Image processing. Micrographs were digitized with a Perkin-Elmer 1010MG flatbed scanning microdensitomer (17) with a raster step corresponding to ~0.3 nm at the specimen. General manipulations of the images were performed with the PIC system (27), which was developed in part from the earlier MDPP system (23). Images (512 by 512 pixels) were displayed for visual inspection on a video monitor with a Gould-DeAnza IP8500 image processor. Photographic negatives of processed images were obtained with the Perkin-Elmer 1010MG in the film-writing mode, with Kodak Shell-Burst type 2476 film and a 50-μm raster.

For correlation averaging and correspondence analysis, programs specifically developed for this purpose were used (T. Pun, M. Unser, B. L. Trus, and A. C. Steven, manuscript in preparation). Of a total of 149 capsomer images that were analyzed, 53 were rejected because they did not converge stably in correlation alignment and 20 were rejected because correspondence analysis showed them to be anomalously (and randomly) different from the bulk of the data set. The remainder were averaged as follows: P-type capsomers (see Fig. 2), $N = 27$; C-type capsomers, $N = 18$; E-type capsomers, $N = 19$; Maltese cross capsomers (not differentiated as to P-, C-, or E-types), $N = 12$. Finally these averaged images were band limited between 0.4 and 0.5 nm^{-1}. As resolution criterion, a phase residual method similar to that of Frank (10) was employed. Cluster analysis (2) of the factoral map of individual capsomer images was performed with C-LAB (M. B. Shapiro and G. D. Knott, *in* D. M. Allen, ed., *Proceedings of the 17th Symposium on the Interface*, in press).

RESULTS

Electron microscopy of partially disrupted HSV-2 nucleocapsids. Micrographs of patches of capsomers derived from capsid facets would be highly suitable for image analysis, because they should lie flat on the support film and thus be viewed in a definite orientation. Furthermore, as monolayers they would greatly reduce the complication of superposition effects. Noting that such patches have previously been obtained in other virus systems (e.g., the groups of nine capsomers of adenovirus (7, 16) and in iridovirus trisymmetrons (32), our experimental strategy was to try to generate corresponding aggregates for HSV-2 by disrupting purified nucleocapsids.

Of the various forms of disruptive treatments that we tried, only limited proteolysis with trypsin gave promising results. In negatively stained preparations, the earliest manifestation of this treatment was the observation of a substantial fraction of particles that had flattened by splitting along their edges, generating a "Maltese cross" appearance (Fig. 1a and b). At slightly later times, isolated patches of capsomers were observed (Figs. 1c and d; see also Fig. 3b). As monitored by sodium dodecyl sulfate-polyacrylamide gel electrophoresis, the time course of tryptic digestion corresponded to gradual conversion of the 155-kilodalton (kDa) capsid protein to major fragments at 85, 82, and 48 kDa (data not shown). The 155-kDa protein is known to be the major capsid protein (6, 12) and is, presumably, the building block of the hexavalent capsomers. However, at the early time points from which our samples for electron microscopy were taken, the extent of proteolysis was slight, and the majority of the 155-kDa protein was still intact. In these experiments, the yield of capsomer patches was small, and our efforts to improve the yields have not been successful. However, we did acquire enough data for image analysis of the capsomer structure.

Optimized image of the hexavalent capsomer of HSV-2. The hexavalent capsomers of a icosahedron with a T number of 16 occupy three distinct bonding environments (Fig. 2): P, those immediately adjacent to a pentavalent capsomer; E, those located on an edge but not vertex adjacent; and C,

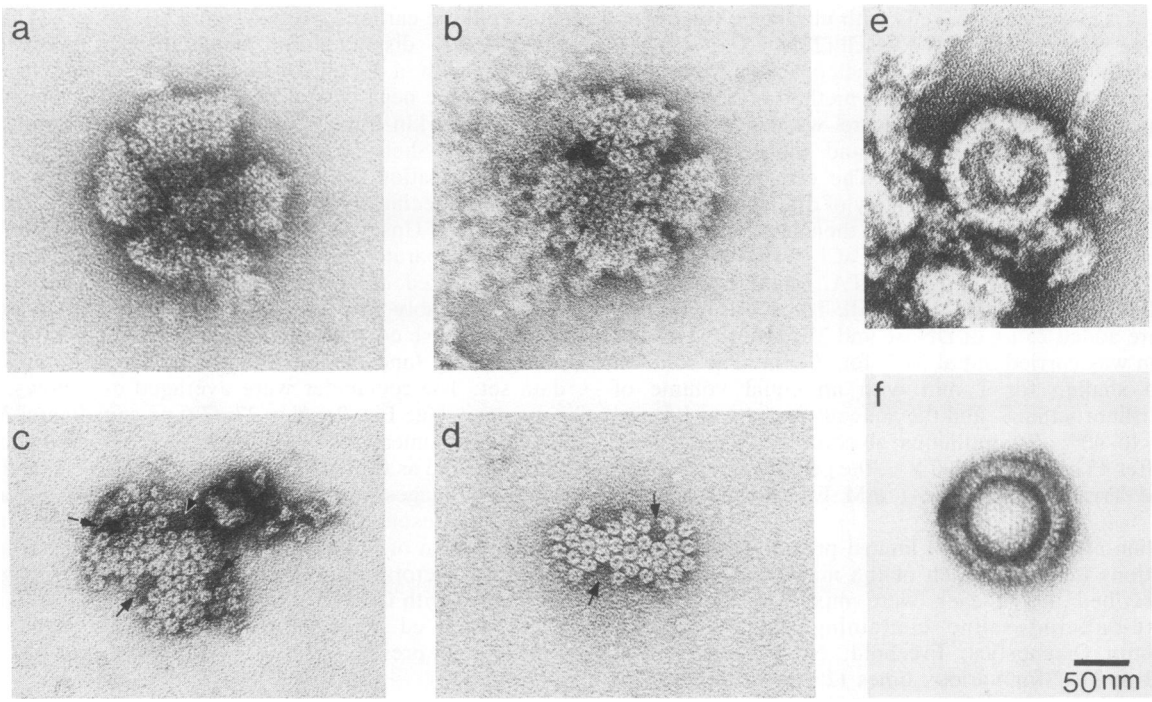

FIG. 1. Electron micrographs of HSV-2 nucleocapsids negatively stained with 1% uranyl acetate. Panels a, b, c, and d represent the respective successive stages of disruption caused by limited proteolysis with trypsin. (a and b) Samples flattened on the electron microscope grid because of splitting along their icosahedral edges, presenting a Maltese cross morphology. (c and d) Monolayer patches of capsomers; arrows indicate the darker staining sites of pentavalent capsomers. (e and f) Intact nucleocapsids penetrated by stain.

those lying in the center of a facet. The average center-to-center spacing of adjacent capsomers was measured to be 12.4 ± 0.6 nm (standard deviation; $N = 89$). Of the 150 hexavalent capsomers, 60 were P, 30 were E, and 60 were C. In principle, the capsomers of these three classes might have different structures, and so our initial analysis treated them separately. This was possible because we were able to identify the positions of pentavalent capsomers in the patches as sites of relatively dense staining (Fig. 1c and d). Whether this property reflects proteolytic degradation of the pentavalent capsomers is not known; nevertheless, it has the useful empirical effect of providing fiducial markers relative to which P, E, and C capsomers may be identified.

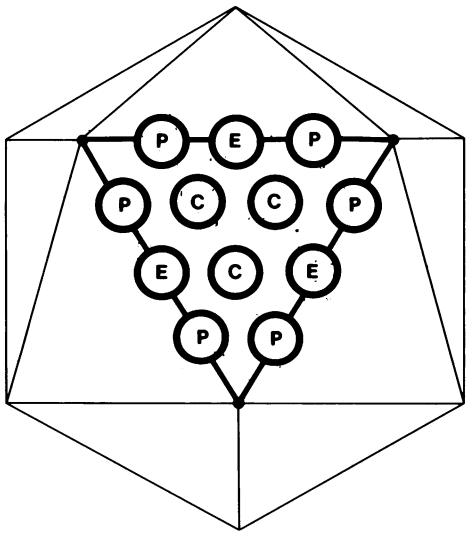

FIG. 2. Schematic diagram of an icosahedron with a T number of 16 viewed along a threefold symmetry axis; the three different types of hexavalent capsomers on a single facet are indicated. They differ in terms of their local bonding environments through their respective configurations of adjacent capsomers and their relative proximities to vertices and edges.

The optimally averaged images of all three capsomer classes are shown in Fig. 3a. The averaging was done in such a way as to compensate for translational displacement of the capsomers from their ideal lattice positions (the average offset encountered was 0.5 nm), and for rotational disordering (the average angular correction was 4.1°). Without this refinement to the averaging technique, smearing of the visualized features of the capsomers would have resulted. In each case (Fig. 3a), the capsomer image has at its center a dense accumulation of stain about 4-nm across and exhibits definite sixfold symmetry. This is most conspicuously seen through the six stained features (presumably surface crevices) that emanate radially from the center. The capsomer images that were combined in each case were oriented in a standard setting relative to a reference frame specified by the nearest vertex site and intervertex line; thus, no rotational averaging was carried out. Consequently, rotational symmetries exhibited in these images must represent real attributes of the capsomers.

From visual appraisal, we found no evident differences among the P, E, and C capsomers (Fig. 3a). In a more quantitative test, the individual images (aligned but not averaged) were analyzed by factorial analysis. This statistical procedure (28) identifies those traits (factors) that exhibit the greatest variability and classifies each image by how those traits are represented in it. A two-dimensional plot is

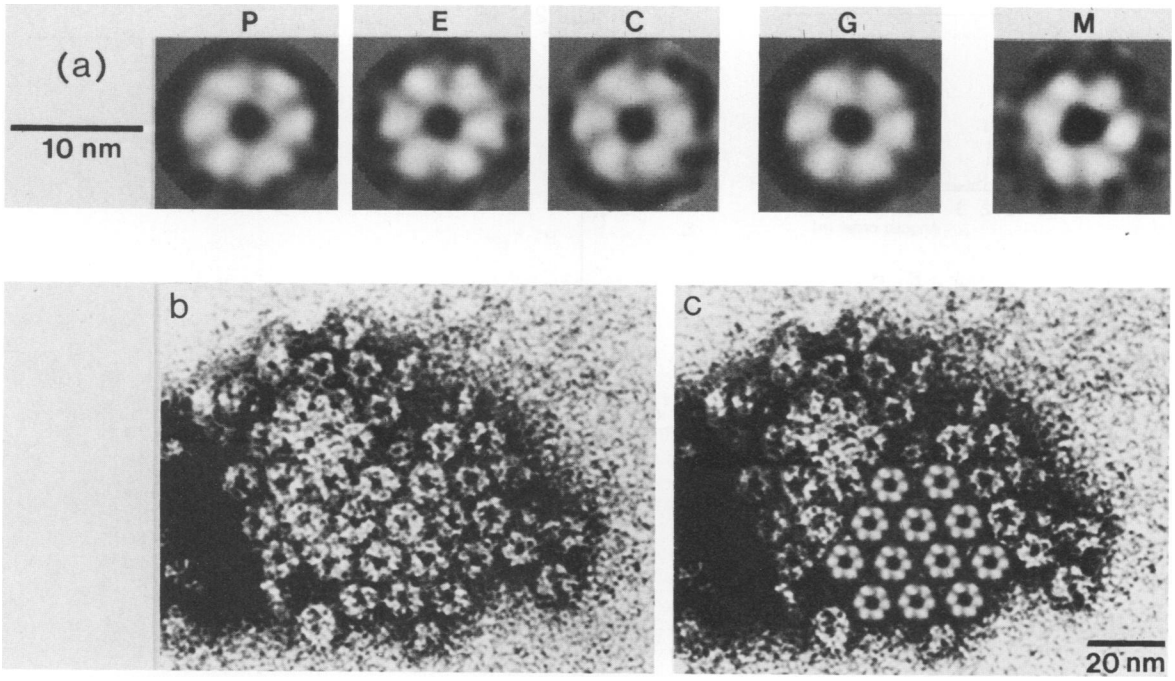

FIG. 3. Computer-processed images of hexavalent HSV-2 capsomers. (a) Optimized images of P, E, and C capsomers, together with the globally averaged (G) image. These images were obtained by correlation averaging of capsomers from monolayer patches. The corresponding image derived from Maltese cross (M) particles is also shown. (b) High-magnification image of a negatively stained patch of capsomers used in this analysis. (c) The same patch as in panel b with processed capsomer image (globally averaged) implanted at the appropriate lattice sites for one icosahedral facet.

presented in Fig. 4 that maps these data by the two most significant factors. If there were to be a statistical trend that distinguished systematically P, E, or C capsomers such a trend would be expressed as a segregation of the capsomer images of a given type into a particular part of this plane. However, no such segregation is evident in Fig. 4, and this conclusion was confirmed quantitatively by cluster analysis (2; Shapiro and Knott, in press). Accordingly, there were no structural differences among them, at least as visualized under these conditions. After this point was established, these data were pooled to amplify the averaging (Fig. 3a, part G). The globally averaged image conveys, with somewhat greater clarity, all the features noted above for the separate images. To confirm that enough averaging had been performed to give an asymptotically stable result, the initial data were randomly divided into two subsets, which were then averaged separately: these images were indistinguishable from each other and from that shown in Fig. 3a, part G.

A similar analysis was conducted with capsomer images derived from a set of Maltese cross images (e.g., Fig. 1a and b), although in this case we were not able to identify the capsomers as types P, E, or C with such confidence. However, this did not appear to matter because the end product was the same in all essential respects as that obtained from the isolated patches (cf. Fig. 3a, parts G and M). We conclude that the projection images of all three hexavalent capsomers (P, E, C) are indistinguishable and that all have unequivocal sixfold symmetry.

Thickness and surface relief of the hexavalent capsomer. To investigate three-dimensional aspects of the capsid structure, we also obtained images of nucleocapsids and nucleocapsid fragments that had been prepared for electron microscopy by freeze-drying and unidirectional shadowing with platinum (Fig. 5). From the lengths of the shadows cast by the flattened structures, we measured the thickness of the capsid shell to be 14.7 ± 1.6 nm (N = 66). The splitting of flattened capsids along their icosahedral edges is illustrated in these images (Fig. 5b to e). The capsid outer surface was studded with conical protrusions, each of which represents a single hexavalent capsomer. On the other hand, the inner surface, when exposed (Fig. 5c, e, and f), presents a relatively smooth and featureless relief. Therefore, the major stain-excluding features visualized by negative staining (Fig. 3b) primarily convey aspects of the outer capsid surface. These inferences with regard to both capsid thickness and the respective reliefs of the inner and outer surfaces are supported by the capsomer side views visualized at the edges of negatively stained nucleocapsids that were infiltrated by stain (Fig. 1e and f). From such images we estimate that the capsid thickness is 15.0 ± 1.5 nm (N = 49). The central channel visualized in Fig. 3 as a feature of heavy stain accumulation and in Fig. 5 as an indentation in the outer surface protrusion is seen to penetrate virtually the entire thickness of the capsomer.

DISCUSSION

In projection, all hexavalent capsomers of HSV-2 have sixfold symmetry. In an earlier study, Furlong (11) examined the rotational power spectra of individual negatively stained herpes simplex type 1 capsomers imaged by scanning transmission electron microscopy. These data suggest that these C capsomers had sixfold symmetry, but were inconclusive with regard to P and E. In this study, our correlation-averaged images of all three types of HSV-2 capsomer exhibited definite sixfold symmetry, both by visual criteria and in terms of their sixfold symmetry residuals which were

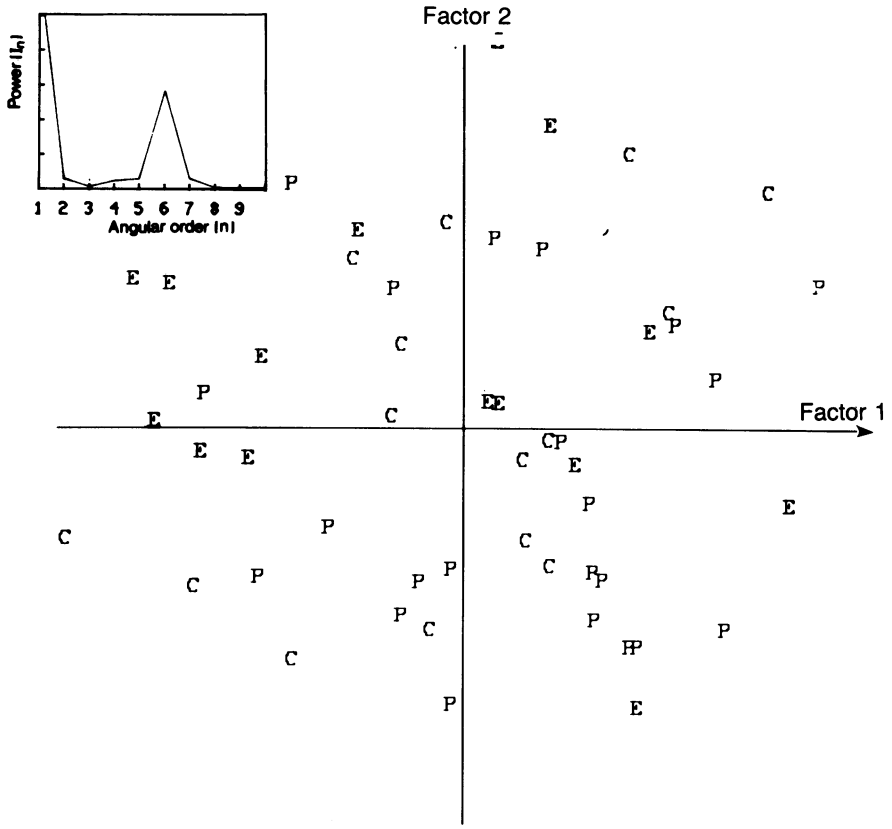

FIG. 4. Two-factor plot of individual images of individual P, E, and C capsomer images classified by correspondence analysis (see text). To improve the signal-to-noise ratios, each image was sixfold symmetrized before analysis. The rotational power spectrum of the global (translational) average capsomer image (Fig. 3a) is inset. The random distribution in the plane of all three types indicates that there are no systematic structural differences among the three types of capsomers, as visualized in this negatively stained data set.

98.0% (P), 97.6% (E), and 98.4% (C) and 99.2% for the globally averaged capsomer. The resolution of these images was ~2.8 nm, according to a phase residual criterion (see above). With our data, we found that the method of rotational power spectrum analysis is inconclusive as applied to individual capsomers. Although some spectra with relatively prominent sixfold harmonics could be found, their significance was unconvincing because of the substantial noise levels and lack of reproducibility. On the other hand, the power spectra of the correlation-averaged images each gave conclusive results (e.g., Fig. 4 inset).

The use of limited proteolysis to generate capsomer patches raises the issue of the structural integrity of the capsomer proteins visualized in these images. It is of interest that tryptic proteolysis of the 155-kDa polypeptide of HSV-2 (albeit a different strain than that used here), indicated that in the dissociated state, the protein could be cleaved into approximately 12 fragments, 7 of which were major (6). In contrast, our trypsinization of this protein in situ generated only three major fragments, suggesting that only a few trypsin-sensitive sites are exposed when the protein is assembled into the capsid. However, our electron microscopic samples were taken at time points when little degradation of the 155-kDa major capsid protein was detected by sodium dodecyl sulfate-polyacrylamide gel electrophoresis. Even if the proteins in the patches were to be partly proteolysed, the cleaved fragments were not necessarily removed; more importantly, the perceived rotational symmetry of the averaged capsomer would not be altered by partial proteolysis, provided only that a random fraction of the monomers was affected. An additional strong argument that inferences drawn from these images are applicable to the intact protein follows from the consistency of the results obtained from the monolayer patches with those obtained from the Maltese cross specimens (Fig. 3a), which were prepared at levels of proteolysis that were barely perceptible by sodium dodecyl sulfate-polyacrylamide gel electrophoresis.

Hexavalent capsomers of HSV-2 are hexamers of the 155-kDa capsid protein. The sixfold symmetry of the capsomer in projection is consistent with its being a hexamer, but it does not completely rule out the alternative possibility that it might be a trimer. For instance, a trimer with three stain-excluding protrusions on its upper surface and three others on the lower surface, offset by an angle of ~30°, would present an apparent sixfold symmetry in projection. However, the markedly different surface reliefs of the upper and lower sides demonstrated in our shadowed specimens (Fig. 5) indicate that the features predominantly contrasted by negative staining are located on the outer surface; on this basis, we reject the trimer hypothesis. An additional argument in favor of the contention that the hexavalent capsomer is indeed a hexamer follows from an estimate of its volume. From two independent types of measurements, we determined that the height of the capsomers was ~15 nm. Their center-to-center spacing was 12.4 nm. Furthermore, from images like that in Fig. 1f, we can

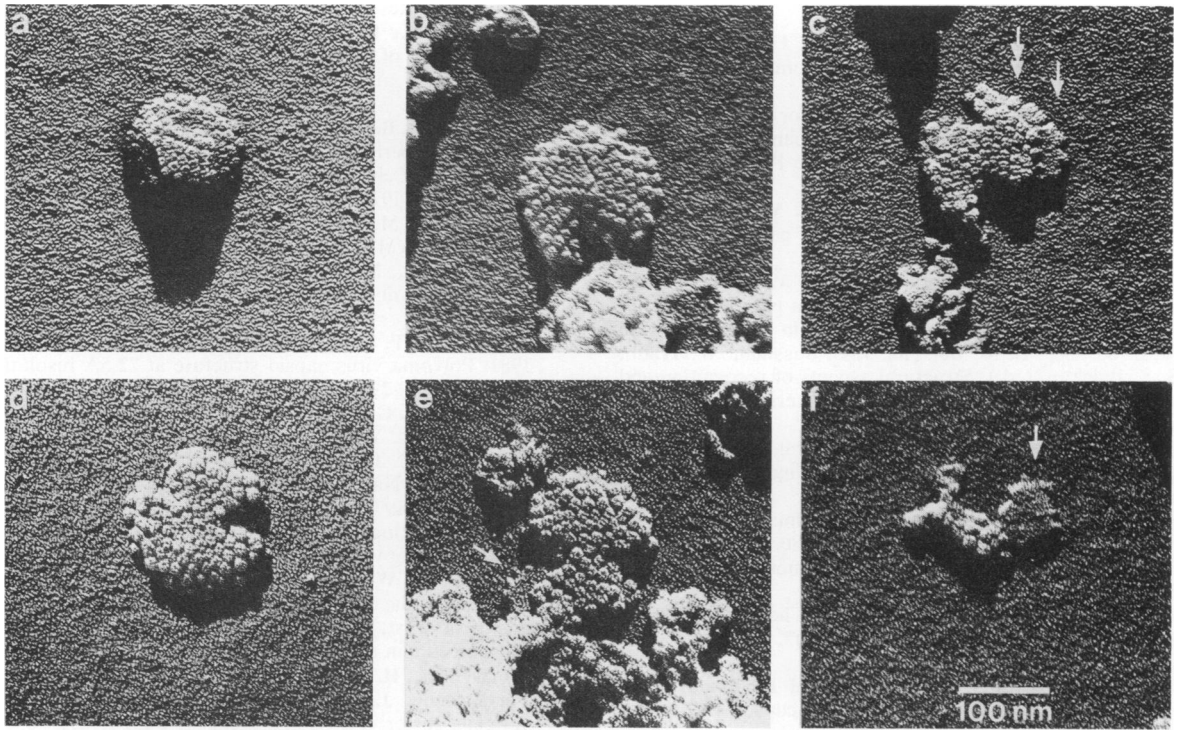

FIG. 5. Electron micrographs of HSV-2 nucleocapsids prepared for electron microscopy by freeze-drying and unidirectional shadowing with platinum. The particles exhibit different degrees of disruption and flattening and different viewing angles. (a) Intact particle viewed along a threefold axis. (b) Flattened particle viewed along a fivefold axis. Particles (b through e) show clear splitting along edges of the icosahedra. In panels c, e, and f, the relatively smooth inner surface of the capsid shell is revealed (white arrows). In panel c, a shadow of double length is cast by an adjacent double layer of capsomers (double-headed arrow).

approximate the dimensions of the hole, which tapers from 4 nm at the outer surface. By calculating the capsomer volume as that of a hollow conical cylinder with the given dimensions and taking the density of protein to be 1.3 g/cm^3, the estimated mass was calculated to be 1,130 kDa, which corresponds to 7.3 copies of the 155-kDa protein. Although there is considerable latitude in this calculation, its result favors the proposition that the capsomer is indeed a hexamer, because to reconcile this value with a trimer would require that our calculation overestimated the volume by a factor of 2.5. On the contrary, precedents indicate that underestimates are generally the case for enclosed molecular volumes calculated by electron microscopic analyses of stained specimens (24).

We conclude that the hexavalent capsomer is a hexamer of the 155-kDa major capsid protein, having the form of a cylindrical cone about 12 nm in diameter and 15 nm in length. It has a deep central indentation about 4-nm wide at the outer surface which tapers progressively toward the base of the capsomer.

An independent estimate of the oligomeric state of the major herpes simplex virus capsid protein follows from the data of Heine et al. (13), who calculated the numbers of copies per virion of the herpes simplex virus type 1 structural proteins based on the molecular weight of the genome, the DNA to protein ratio, and estimates of the relative amounts of the proteins from quantitation of Coomassie blue-stained gels and autoradiograms of ^{14}C-labeled preparations. Insertion of the more recent value for the genome mass of 97 ± 5 megadaltons (30) into their calculation gives quotas of 824 ± 41 (Coomassie blue stain) and 970 ± 50 (^{14}C-labeling) per virion of the 155-kDa major capsid protein. According to the hexamer hypothesis, there should be 900 copies if the pentavalent capsomers consist of some other protein(s), and 960 copies if they are pentamers of the same protein. According to the trimer hypothesis, there should be 450 copies if the pentavalent capsomers consist of some other protein(s), and 486 if they are also trimers of the 155-kDa protein. Although the uncertainties attributed to the biochemical quantitations (13) appear to be underestimates, these data agree that the hexavalent capsomers are hexamers.

Molecular implications of symmetry-breaking in HSV capsid (expression of quasi-equivalence). Our results have shown that the structures of P, E, and C capsomers of HSV-2 are essentially the same when visualized in planar arrays of capsomer patches (Fig. 3a). However, in the unflattened icosahedral capsid, it is clear that the dissimilarities between their respective bonding environments must be reflected in substantially different structural arrangements. In particular, P and E (cf. Fig. 2) lie along edges of the icosahedron and must presumably be symmetrically disposed relative to the two facets which meet at the edge; consequently, they must be tilted or distorted to some considerable extent relative to the conformation of C. As yet, we have no insight into how such distortions are accommodated at the molecular level. Similarly, the molecular identity and oligomeric nature of the pentavalent capsomers remain to be solved.

ACKNOWLEDGMENT

We thank Michael Unser for helpful discussions about image processing and correspondence analysis.

LITERATURE CITED

1. **Almeida, J., D. Lang, and P. Talbot.** 1978. Herpesvirus morphology; Visualisation of a structural subunit. Intervirology, **10**:318–320.
2. **Anderberg, M. R.** 1973. Cluster analysis for applications. *In* Z. W. Birnbaum and E. Lukacz (ed.), Probability and mathematical statistical series, vol. 19. Academic Press, Inc., New York.
3. **Baker, T. S., D. L. D. Caspar, and W. T. Murakami.** 1983. Polyoma virus "hexamer" tubes consist of paired pentamers. Nature (London) **303**:446–448.
4. **Burnett, R. M., M. C. Grutter, and J. L. White.** 1981. The molecular structure of hexon, the major coat protein of adenovirus—its placement and its interactions in the icosahedral capsid, p. 865–868. *In* M. Balaban, J. L. Sussman, W. Traub, and S. S. Balaban, (ed.), Structural aspects of recognition and assembly in biological macromolecules. International Science Services, Rehovot, Israel.
5. **Caspar, D. L. D., and A. Klug.** 1962. Physical principles in the construction of regular viruses. Cold Spring Harbor Symp. Quant. Biol. **27**:1–24.
6. **Cohen, G. H., M. Ponce de Leon, H. Diggelman, W. C. Lawrence, S. L. Vernon, and R. J. Eisenberg.** 1980. Structural analysis of the capsid polypeptides of herpes simplex virus types 1 and 2. J. Virol. **34**:521–531.
7. **Crowther, R. A., and R. M. Franklin.** 1972. The structure of the groups of nine hexons from adenovirus. J. Mol. Biol. **68**:181–184.
8. **Devaux, C., M. Zulauf, P. Boulanger, and B. Jacrot.** 1983. Molecular weight of adenovirus serotype 2 capsomers. A new characterization. J. Mol. Biol. **156**:927–939.
9. **Frank, J.** 1975. Averaging of low-exposure electron micrographs of non-periodic objects. Ultramicroscopy **1**:159–162.
10. **Frank, J., A. Verschoor, and M. Boublik.** 1981. Computer averaging of electron micrographs of 40S ribosomal subunits. Science **214**:1353–1355.
11. **Furlong, D.** 1978. Direct evidence for 6-fold symmetry of the herpesvirus hexon capsomere. Proc. Natl. Acad. Sci. USA **75**:2764–2766.
12. **Gibson, W., and B. Roizman.** 1974. Proteins specified by herpes simplex virus. X. Staining and radiolabeling properties of B capsid and virion proteins in polyacrylamide gels. J. Virol. **13**:155–165.
13. **Heine, J. W., R. W. Honess, E. Cassai, and B. Roizman.** 1974. Proteins specified by herpes simplex virus. XII. The virion peptides of type 1 strains. J. Virol. **14**:640–651.
14. **Kistler, J., U. Aebi, and E. Kellenberger.** 1977. Freeze-drying and shadowing a two-dimensional periodic specimen. J. Ultrastruct. Res. **59**:76–86.
15. **Labaw, L., and D. R. Davies.** 1972. The molecular outline of human γG1 immunoglobulin from an EM study of crystals. J. Ultrastruct. Res. **401**:349–365.
16. **Maizel, J. V., D. O. White, and M. D. Scharff.** 1968. The polypeptides of adenovirus. II. Soluble proteins, cores, top components and the structure of the virion. Virology **36**:126–136.
17. **McGee, P. E., B. L. Trus, and A. C. Steven.** 1982. Techniques to evaluate the performance of scanning microdensitometers in the digitization of electron micrographs. Micron **13**:221–228.
18. **Misell, D. L.** 1978. Image analysis, enhancement and interpretation. *In* A. M. Glauert (ed.), Practical methods in electron microscopy, vol. 7. North Holland, Amsterdam.
19. **Palmer, E. L., M. Martin, and G. W. Gary.** 1975. The ultrastructure of disrupted herpesvirus nucleocapsids. Virology **65**:260–265.
20. **Rayment, I., T. S. Baker, D. L. D. Caspar, and W. Murakami.** 1981. Polyoma virus capsid structure at 22.5Å resolution. Nature (London) **295**:110–115.
21. **Rossmann, M. G.** 1984. Constraints on the assembly of spherical virus particles. Virology **36**:1–11.
22. **Russell, W. C.** 1962. A sensitive and precise plaque assay for herpes virus. Nature (London) **195**:1028–1029.
23. **Smith, P. R.** 1978. An integrated set of computer programs for processing electron micrographs of biological structure. Ultramicroscopy **3**:153–160.
24. **Smith, P. R., W. E. Fowler, T. D. Pollard, and U. Aebi.** 1983. Structure of the actin molecule determined from electron micrographs of crystalline actin sheets with a tentative alignment of the molecule in the actin filament. J. Mol. Biol. **165**:641–660.
25. **Straus, S. E., H. Aulakh, W. T. Ruyechan, J. Hay, T. Casey, G. Vandewoude, J. Owens, and H. Smith.** 1981. Structure of varicella zoster virus DNA. J. Virol. **40**:516–525.
26. **Timbury, M. C.** 1971. Temperature-sensitive mutants of herpes simplex virus type 2. J. Gen. Virol. **13**:373–376.
27. **Trus, B. L., and A. C. Steven.** 1981. Digital image processing of electron micrographs—the PIC system. Ultramicroscopy **6**:383–386.
28. **Van Heel, M., and J. Frank.** 1981. Use of multivariate statistics in analysing the images of biological macromolecules. Ultramicroscopy **6**:187–194.
29. **Vernon, S. K., W. C. Lawrence, and G. H. Cohen.** 1974. Morphological components of herpesvirus. I. Intercapsomeric fibrils and the geometry of the capsid. Intervirology **4**:237–248.
30. **Wadsworth, S. C., R. J. Jacob, and B. Roizman.** 1975. Anatomy of herpes simplex virus DNA. II. Size, conformation, and arrangement of inverted terminal repeats. J. Virol. **15**: 1487–1497.
31. **Wildy, R., W. C. Russell, and R. W. Horne.** 1960. The morphology of herpes virus. Virology. **12**:204–222.
32. **Wrigley, N. G.,** 1969. An electron microscope study of the structure of sericesthis iridescent virus. J. Gen. Virol. **9**:123–134.